



ACADEMIC  
PRESS

Available online at [www.sciencedirect.com](http://www.sciencedirect.com)

SCIENCE @ DIRECT®

Journal of Sound and Vibration 263 (2003) 549–567

JOURNAL OF  
SOUND AND  
VIBRATION

[www.elsevier.com/locate/jsvi](http://www.elsevier.com/locate/jsvi)

# Large motion tracking control for thrust magnetic bearings with fuzzy logic, sliding mode, and direct linearization

T.P. Minihan<sup>a,\*</sup>, S. Lei<sup>a</sup>, G. Sun<sup>a</sup>, A. Palazzolo<sup>a</sup>, A.F. Kascak<sup>b</sup>, T. Calvert<sup>c</sup>

<sup>a</sup>Department of Mechanical Engineering, Texas A&M University, MS 3123, College Station, TX 77843-3123, USA

<sup>b</sup>US Army at NASA Glenn, Cleveland, Oh, USA

<sup>c</sup>Naval Surface Warfare Center, Carderock Division, Philadelphia, PA, USA

Received 21 August 2000; accepted 18 June 2002

---

## Abstract

Conventional use of magnetic bearings relies on a zero reference to keep the rotor centered in the radial and axial axes. This paper compares different control methods developed for the alternate control task of tracking an axial dynamic target. Controllers based on fuzzy logic, sliding mode, and direct linearization were designed to meet this task. Performance criteria, such as maximum axial displacement, minimum phase lag and  $I^2R$  power losses were compared for each controller. The large motion, tracking problem for a rotor has utility in applications where dynamic seal clearances are required. This has a variety of potential applications in turbo-machinery, such as active stall control.

© 2002 Elsevier Science Ltd. All rights reserved.

---

## 1. Introduction

Active magnetic suspension technology has found a wide range of applications in recent years. Basically, these applications fall into two categories: those using large air gaps, such as wind tunnel model suspensions, and those using small air gaps such as magnetic bearings in fast rotating systems. The development of magnetic bearings in rotating machinery has increased significantly due to their low-power loss and high-speed operation. Since the shaft and the bearing assembly have no contact between one another, frictional loss, which grows drastically with speed increase, is greatly reduced. Active magnetic bearings require closed-loop feedback, which offers a way to support the rotating shaft as well as to control the vibration. In most industrial applications, the feedback system includes a linear PID controller with compensators, power

---

\*Corresponding author. Tel.: +1-979-845-4580; fax: +1-979-862-2892.

E-mail address: [tminihan@tamu.edu](mailto:tminihan@tamu.edu) (T.P. Minihan).

amplifiers, magnetic actuators and inductive, eddy current or optical sensors [1]. In addition to the widely applied PID controllers, advanced control strategies such as optimal control [2],  $\mu$ -synthesis control [3],  $H$ - $\infty$  control [4,5] can be found in some applications. All these methods are based on linear systems theory and require linear models. Non-linear control techniques were also applied to active magnetic bearings. Sliding mode control [6–8] and fuzzy-logic-based control [9,10] can be found in several papers, but are limited to regulator (static target) applications. A sliding mode controller [8] for thrust magnetic bearing was designed and verified by experiment for two rotor trajectories: an overdamped second order system of frequency 20 rad/s and a 2 Hz sinusoidal signal of 0.1 mm amplitude.

The purpose of this research is to develop robust, non-linear controllers for active magnetic bearings and to show their advantages over linear, PID controllers for tracking a sinusoidal reference in the axial direction. A PID controller was initially designed to accomplish this, however, the desired large amplitudes could not be obtained and substantial phase lags resulted. Three types of non-linear controllers were then investigated: fuzzy logic integrated with PD control, sliding mode, and direct linearization. Each controller was simulated with identical plant, actuators, and closed-loop system. A comparison of the three controllers was made based on the performance characteristics; tracking accuracy, power losses, phase lag, and computation demand. In addition to providing a comparison between the three methods the paper provides an original contribution for high-frequency, large target motion tracking control.

## 2. Plant, actuator and sensor models

The plant consists of a rigid rotor suspended on a five-axis magnetic bearing system as shown in Fig. 1. Only axial motion is considered in this study and it is actuated by the thrust bearing shown in Fig. 2. The total current is a combination of bias current  $i_0$  and control current  $i_c$ , and circulates through coils on the thrust bearing stator.

Material reluctance was included in the flux path models for the stator and rotor. The resulting expression for flux density in the opposed electromagnets is expressed in Eq. (1) and is derived

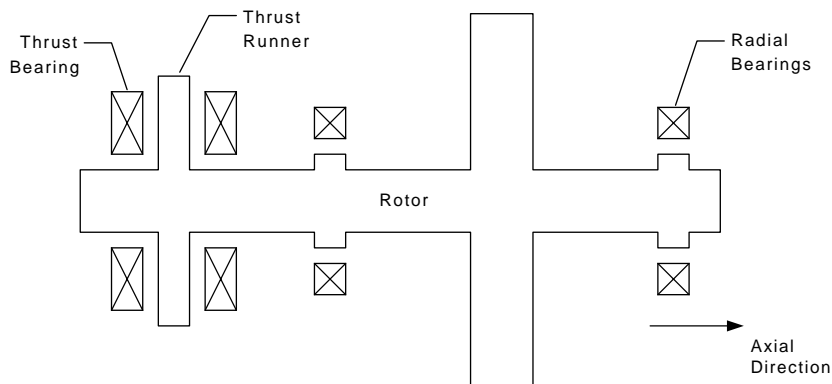


Fig. 1. Typical magnetic suspension system for a rotor.

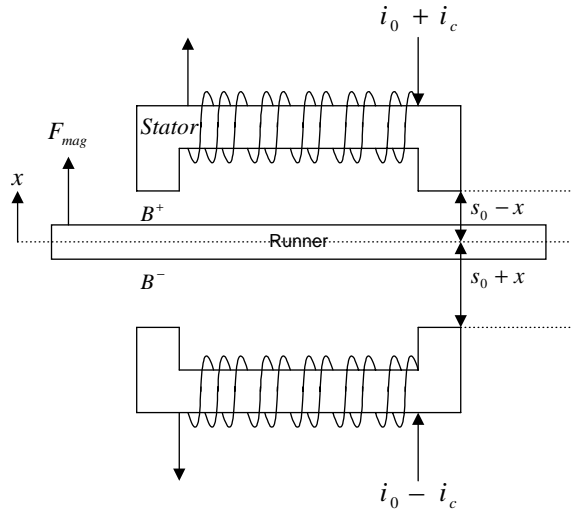


Fig. 2. Typical thrust bearing geometry with displacement and current variables.

from Ampere’s Law:

$$B^\pm = \frac{Ni^\pm}{(L_{stator}/\mu_{stator} + L_{rotor}/\mu_{rotor} + 2(s_0 \mp x/\mu_0))}, \tag{1}$$

where  $s_0$  is the nominal air gap between rotor and magnetic bearing,  $L_{stator}$  and  $L_{rotor}$  are the lengths of the flux paths in the stator and rotor, respectively,  $\mu_{stator}$  and  $\mu_{rotor}$  are the permeability of the stator and rotor, respectively, and  $\mu_0$  is the permeability of air in free space.

The magnetic force per pole pair is given below, where  $B$  is the flux density,  $f$  is the fringe factor,  $A_p$  is the pole area. This represents the magnetic force per pole pair, assuming two air gaps per pair:

$$F_{mag} = \frac{(fB)^2 A_p}{\mu_0}. \tag{2}$$

A fringe factor  $f$  of 0.8 was used to account for fringing effects. A piecewise linear approximation for the stator and rotor material  $B$ – $H$  curve was used to represent permeability and saturation characteristics.

Substituting Eq. (1) into Eq. (2), the equations of axial motion for the rotor due to the magnetic force can be expressed as

$$m\ddot{x} = \sum F_{mag} = kf^2 \left[ \frac{(i_0 + i_c)^2}{(s_0 - x)^2} - \frac{(i_0 - i_c)^2}{(s_0 + x)^2} \right], \tag{3}$$

where  $k = A_p N_2 \mu_0 N_c / 4$ ,  $N_c$  is the number of  $c$ -cores for one stator,  $i_0$  is the bias current, and  $i_c$  is the control current from the power amplifier.

Power amplifiers drive current through the actuator coils and are modelled with voltage and current saturation due to the inductive and resistive electrical loads. A current servo loop was also included in the power amplifier model with a bandwidth of 2500 Hz. The open-loop transfer

function for the power amplifier is written as

$$G_{PA} = K_{PA} \frac{1}{(Ls + R)}, \tag{4}$$

where  $K_{PA}$  is the current servo feedback gain and  $L$  and  $R$  are the inductance and resistance of one coil, respectively. The  $K_{PA}$  current sensor servo feedback gains are adjusted to obtain the desired bandwidth and DC gain (1 A/V).

The actuators (opposed electromagnets) were modelled with a 1000 Hz cutoff frequency ( $f_a$ ) based on finite element field simulations. The actuator transfer function is

$$G_{act} = \frac{1}{(\tau_a s + 1)}, \tag{5}$$

where  $\tau_a = 1/(2\pi f_a)$ .

Sensor dynamics are modelled as

$$G_{sen} = \frac{\xi_s}{(\tau_s s + 1)}, \tag{6}$$

where the sensitivity is  $\xi_s = 7874$  V/m, the cutoff frequency is  $f_s = 3000$  Hz; and  $\tau_s = 1/(2\pi f_s)$ . A closed-loop block diagram of the axial magnetic bearings system is illustrated in Fig. 3. The total current in each actuator consists of a bias current and control current with the control current equal and opposite between the two actuators.

Fig. 4 shows the non-linear relationship between the magnetic force and total current. This also shows the inertial force that results with a zero to peak displacement of  $1.27 \times 10^{-4}$  m (33% of the air gap) and frequency of 150 Hz. The remaining parameter values are  $m = 22.6$  kg and  $k = 5.065 \times 10^{-6}$  N m<sup>2</sup>/A<sup>2</sup>. Some notable features of Fig. 4 are: (1) the magnetic force is clearly

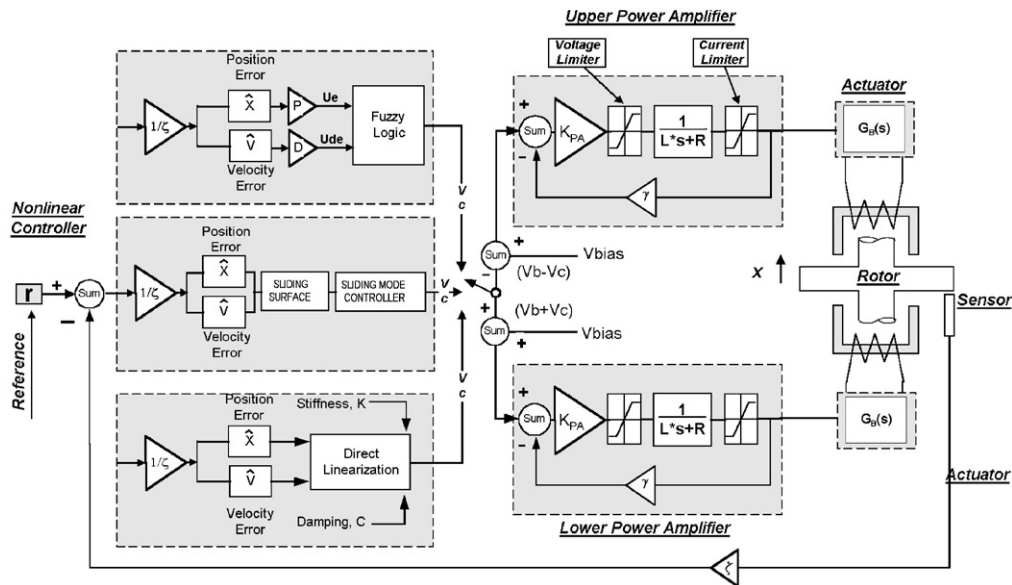


Fig. 3. Closed-loop system.

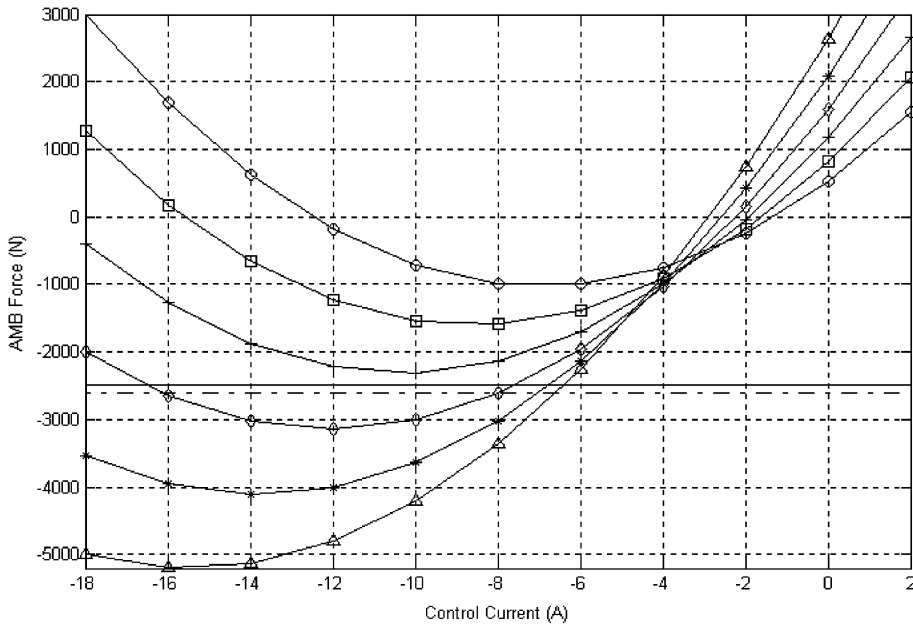


Fig. 4. Actuator force versus control current with  $X_{amplitude} = 1.27 \times 10^{-4}$  m: o, 4 A; □, 5 A; +, 6 A; ◇, 7 A; \*, 8A; Δ, 9A.

non-linear and has a distinct peak versus control current, for a fixed bias current; (2) the peak negative force (load capacity) varies significantly with bias current; (3) a certain minimum level of bias current is required to balance the inertial force; (4) the force cannot exceed that which occurs ( $F_{sat}$ ) when one actuator stator is fully saturated and the other is flux free, with  $B_{sat} = 1.8$  T.

A control objective is to track a 150 Hz displacement reference of  $1.27 \times 10^{-4}$  m sinusoidal amplitude:

$$X_{amplitude} = 1.27 \times 10^{-4} \text{ m.} \tag{7}$$

The required force amplitude according to Newton’s law must be

$$F_{inertial} = -m(X_{amplitude})(2\pi f_{sh})^2, \tag{8}$$

where  $f_{sh}$  is the shaking frequency. The magnetic force must be sufficient to balance the inertial force:

$$\max|F_{mag}| > |F_{inertial}| = 2481.8 \text{ N,} \tag{9}$$

which is independent of the control algorithm. Eq. (3) is used to plot the control current  $i_c$  as a function of  $X_{amplitude}$ , with the bias current  $i_0$  as a parameter. Given the  $X_{amplitude}$ , Fig. 5 may be employed to estimate the bias and control current requirements for the preliminary design of the actuator. For example, if  $X_{amplitude} = 1 \times 10^{-4}$  m and the bias current is 5 A, then from Fig. 5  $i_c = 9.5$  A. On the other hand, if  $X_{amplitude} = 1 \times 10^{-4}$  m and the bias current is 4 A, then the target displacement cannot be obtained, for the given shake frequency (150 Hz) and rotor mass.

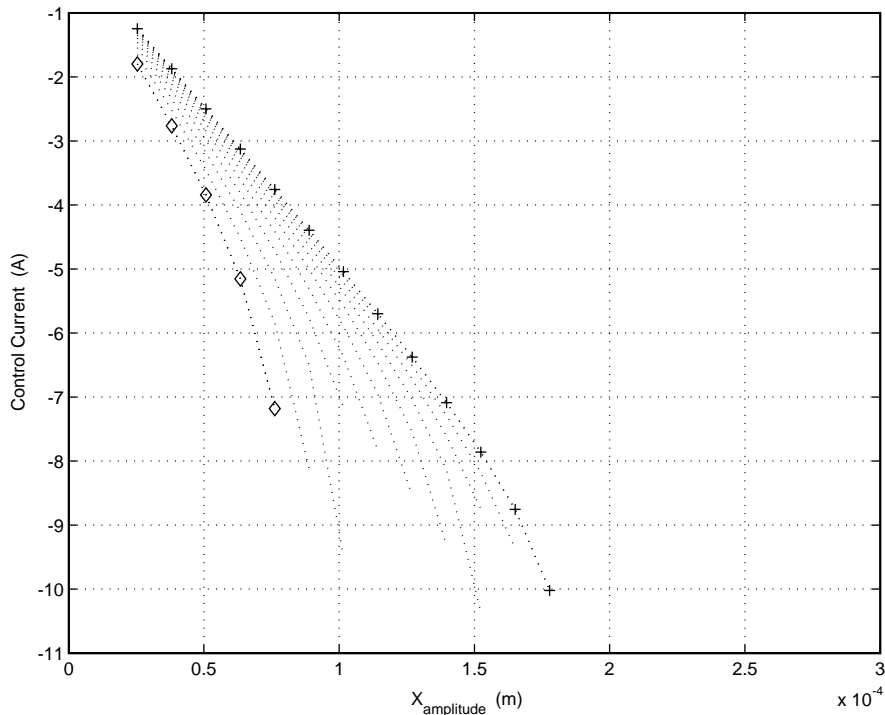


Fig. 5. Required control current as a function of desired displacement and bias current, at  $f_{sh} = 150$  Hz:  $\diamond$ , 4 A bias current;  $\cdots$  intermediate values; +, 10 A bias current.

### 3. Controller theory and model

#### 3.1. Fuzzy logic control for tracking

Fuzzy logic theory was first established in Zadeh's seminal paper in 1965 [11]. Mamdani applied fuzzy logic to dynamics [12] about 10 years later. The Mamdani architecture of a fuzzy logic controller is based on qualitative and empirical knowledge of human beings. Later Takagi and Sugeno established a fuzzy model, called the Takagi–Sugeno model [13], which can be more easily used for analytical purposes. A Mamdani architecture is used here to build a non-linear rule-based fuzzy logic control system. Fuzzy logic controllers for active magnetic bearings are synthesized and designed for stabilizing the system during the command following process. The antecedent and consequent of each rule are defined in terms of input and output variables in predefined membership functions. These membership functions possess qualitative descriptions, which generalize the notion of assigning a single degree to a specific response severity or corrective action level. The rule base is constructed to provide a non-linear resistance with respect to the position error of the rotor. The purpose of this is to compensate for the electromagnetic force  $F_{mag}$ , Eq. (3), which is non-linear in both the displacement  $x$  and the active control current  $i_c$  (see Figs. 4 and 5).

In order to design a fuzzy logic rule base, it is necessary to investigate how the runner responds to the control signal. When the error signal  $e = x_d - x > 0$ , where  $x_d$  is the desired input, positive

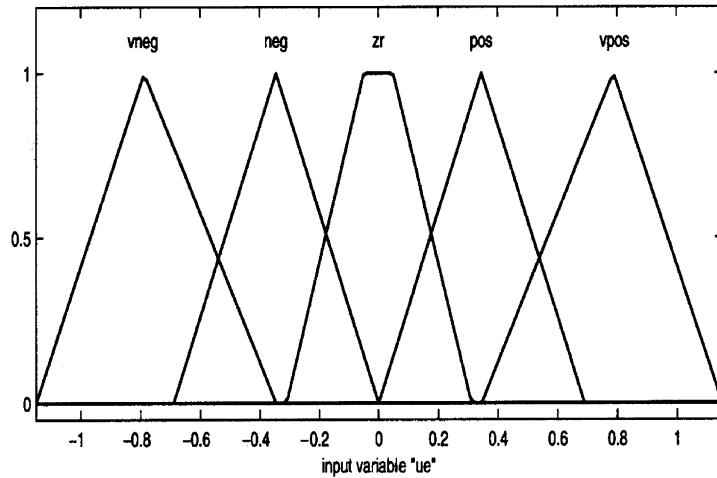


Fig. 6. Input *ue* membership function in MATLAB GUI.

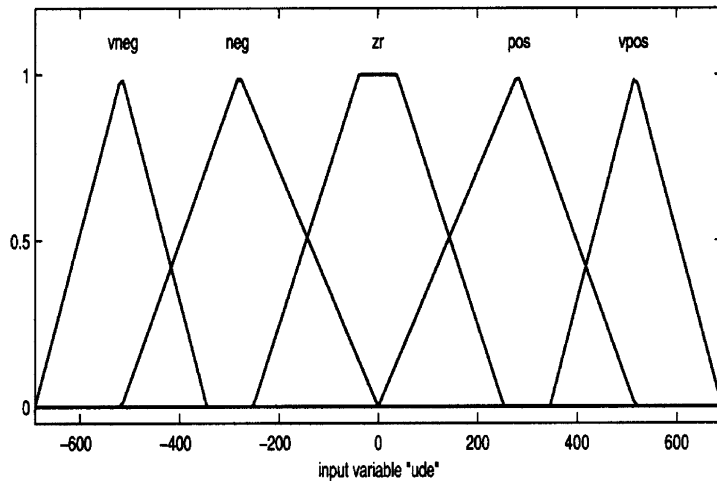


Fig. 7. Input membership function *ude* in MATLAB GUI.

control current  $i_c > 0$  is required to further move the runner toward the desired position. On the other hand, when the error signal  $e = x_d - x < 0$ , negative control current  $i_c < 0$  is required. Analogous logic is used to formulate all membership functions and the entire rule base. Figs. 6 and 7 show two input membership functions: error voltage (*ue*) and change-of-error voltage (*ude*), which correspond to the proportional and derivative parts of the error, respectively.

Fig. 8 shows the output membership function which consists of five triangular sets. The rule base is shown in Fig. 9 and has 25 rules. The output *ctrl* is a control voltage to the power amplifiers.

### 3.2. Sliding mode control for tracking

Next, a sliding mode control (SMC) or so-called switching control [14] is applied to axial motion tracking of a rotor AMB system. This control method can be applied to non-linear system

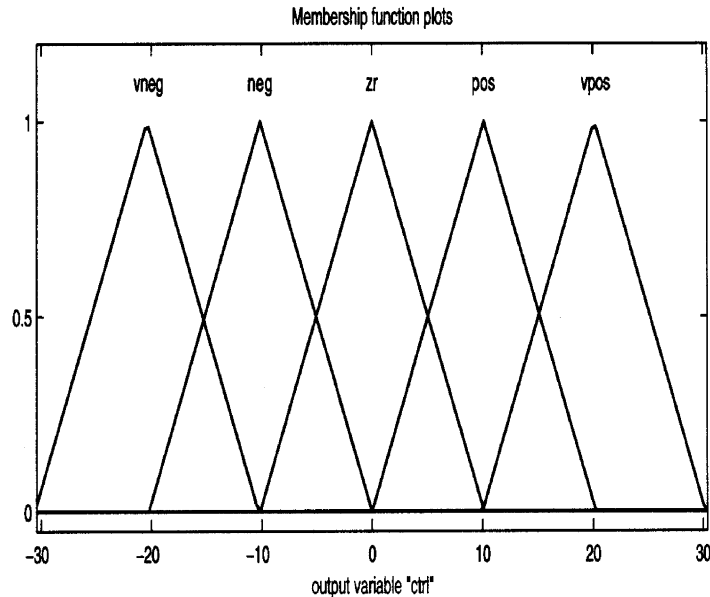


Fig. 8. Output membership function *ctrl* in MATLAB GUI.

1. If (ue is vneg) and (ude is vneg) then (ctrl is vneg) (1)
2. If (ue is vneg) and (ude is neg) then (ctrl is vneg) (1)
3. If (ue is vneg) and (ude is zr) then (ctrl is neg) (1)
4. If (ue is vneg) and (ude is pos) then (ctrl is zr) (1)
5. If (ue is vneg) and (ude is vpos) then (ctrl is zr) (1)
6. If (ue is neg) and (ude is vneg) then (ctrl is vneg) (1)
7. If (ue is neg) and (ude is neg) then (ctrl is vneg) (1)
8. If (ue is neg) and (ude is zr) then (ctrl is neg) (1)
9. If (ue is neg) and (ude is pos) then (ctrl is zr) (1)
10. If (ue is neg) and (ude is vpos) then (ctrl is zr) (1)
11. If (ue is zr) and (ude is vneg) then (ctrl is neg) (1)
12. If (ue is zr) and (ude is neg) then (ctrl is neg) (1)
13. If (ue is zr) and (ude is zr) then (ctrl is zr) (1)
14. If (ue is zr) and (ude is pos) then (ctrl is pos) (1)
15. If (ue is zr) and (ude is vpos) then (ctrl is pos) (1)
16. If (ue is pos) and (ude is vneg) then (ctrl is zr) (1)
17. If (ue is pos) and (ude is neg) then (ctrl is zr) (1)
18. If (ue is pos) and (ude is zr) then (ctrl is pos) (1)
19. If (ue is pos) and (ude is pos) then (ctrl is vpos) (1)
20. If (ue is pos) and (ude is vpos) then (ctrl is vpos) (1)
21. If (ue is vpos) and (ude is vneg) then (ctrl is zr) (1)
22. If (ue is vpos) and (ude is neg) then (ctrl is zr) (1)
23. If (ue is vpos) and (ude is zr) then (ctrl is pos) (1)
24. If (ue is vpos) and (ude is pos) then (ctrl is vpos) (1)
25. If (ue is pos) and (ude is vpos) then (ctrl is vpos) (1)

Fig. 9. The rule base for fuzzy logic control.

in the presence of uncertain parameters provided that the upper bounds of the uncertain parameters are known. SMC design consists of two steps: (1) define the sliding surface upon which the system has the desired stability and tracking properties, and (2) design the non-linear

controller gain for driving the system to the sliding surface and making it remain there using the sliding condition from the Lyapunov stability theorem.

The time-varying sliding surface  $s$  for  $n$ th order system is defined by scalar function

$$s(X, t) = \left( \frac{d}{dt} + \lambda \right)^{n-1} \tilde{x}, \tag{10}$$

where  $X(t) = [x, \dot{x}, \dots, x^{(n-1)}]^T$  is the state vector,  $\tilde{x} = x - x_d$ ,  $x$  is the state of given system,  $x_d$  is the desired input,  $\lambda$  is strictly positive, and  $n$  is the order of system. For the second order system,

$$s = \left( \frac{d}{dt} + \lambda \right) \tilde{x} = \dot{\tilde{x}} + \lambda \tilde{x}. \tag{11}$$

Based on the Lyapunov stability theorem, the so-called sliding condition for stability can be defined as

$$\frac{1}{2} \frac{d}{dt} (s^2(X, t)) \leq -\eta |s| \leq 0, \tag{12}$$

where  $\eta$  is a strictly positive constant. Differentiate both sides of Eq. (11) and substitute Eq. (3):

$$\dot{s} = \ddot{\tilde{x}} + \lambda \dot{\tilde{x}} = \ddot{x} - \ddot{x}_d + \lambda \dot{\tilde{x}} = \frac{1}{m} F_{mag} - \ddot{x}_d + \lambda \dot{\tilde{x}}. \tag{13}$$

It is assumed that the force constant  $k$  from Eq. (3) is uncertain. This uncertain parameter is extracted from  $F_{mag}$ ,

$$\dot{s} = \frac{k}{m} F_k - \ddot{x}_d + \lambda \dot{\tilde{x}}, \tag{14}$$

where  $F_k = F_{mag}/k$ . Let  $k/m$  equal  $b$ , and then the nominal  $F_k$ ,  $\hat{F}_k$  to make  $\dot{s} = 0$  is obtained from Eq. (14) as

$$\hat{F}_k = \hat{b}^{-1}(\ddot{x}_d - \lambda \dot{\tilde{x}}). \tag{15}$$

It is assumed that  $b$  can be bounded by the inequality

$$0 < b_{min} \leq b \leq b_{max}. \tag{16}$$

The geometric mean of  $b$  is selected for the estimated gain  $b$ ,  $\hat{b}$ . From the definition of geometric mean,

$$\hat{b} = (b_{min} b_{max})^{1/2}. \tag{17}$$

Let  $\Delta$  be the maximum error, which exists between the uncertain value  $k$  and the nominal value,  $\hat{k}$ , and then inequality (16) can be written in the form

$$\frac{1}{\beta} \leq \left( \frac{\hat{b}}{b} \right) \leq \beta, \tag{18}$$

where  $\beta = \sqrt{(1 + \Delta)/(1 - \Delta)}$ . The following sliding mode controller is obtained by adding a discontinuous term across the sliding surface  $s = 0$  to Eq. (15):

$$F_k = \hat{b}^{-1}(\ddot{x}_d - \lambda \dot{\tilde{x}} - \xi \text{sat}(s/\Phi)), \tag{19}$$

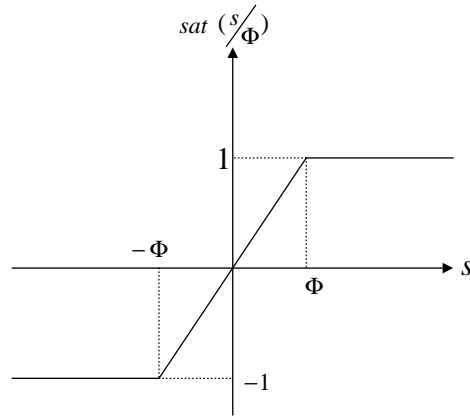


Fig. 10. Discontinuous function in sliding mode controller.

where  $\xi$  is the controller gain and  $\Phi$  is the boundary layer thickness of saturation function  $sat(\cdot)$  shown in Fig. 10. The discontinuous term is added for the purpose of making the sliding surface approach  $s = 0$  and remain there, compensating for the imperfection of the estimated force in Eq. (15). Substituting Eq. (19) into inequality (12) and applying inequality (18) the following controller gain is obtained:

$$\xi = |1 - \beta| |\ddot{x}_d - \lambda \dot{x}| + \beta \eta. \tag{20}$$

From the non-linear magnetic force Eq. (3),

$$F_k = f^2 \left[ \frac{(i_o + i_c)^2}{(s_o - x)^2} - \frac{(i_o - i_c)^2}{(s_o + x)^2} \right]. \tag{21}$$

The control current,  $i_c$ , is directly solved from Eq. (21),

$$i_c = \left[ -i_o(s_o^2 + x^2) + (s_o^2 + x^2) \sqrt{i_o^2 + F_k/f^2 s_o x} \right] / (2s_o x). \tag{22}$$

In the case that  $x = 0$  (singular point of Eq. (22)),

$$i_c = F_k / K_I, \tag{23}$$

where  $K_I = 4f^2(i_o/s_o^2)$ .

### 3.3. Direct linearization control for tracking

This controller’s strategy is to produce a closed loop control force which is linearly proportional to the tracking error and error rate. The non-linear magnetic force equation (3) is equated to a first order linear expression based on rotor position and velocity error:

$$F_{desired} = C \dot{\tilde{x}} + K \tilde{x}, \tag{24}$$

where  $\tilde{x} = x - x_d$ ,  $\tilde{x}$  and  $\dot{\tilde{x}}$  are the tracking errors and  $C$  and  $K$  are damping and spring constants realized actively via the feedback control. The required control current is from Eq. (3):

$$i_c = \frac{i_0}{2s_0x} \left\{ -(s_0^2 + x^2) + (s_0^2 - x^2) \sqrt{1 + \frac{4s_0x}{f^2 i_0^2 N^2 A_p \mu_0} (C\dot{\tilde{x}} + K\tilde{x})} \right\}. \quad (25)$$

Since this expression is undefined for zero position, the quadratic equation must be solved again to yield the correct control current under this condition

$$i_c = \frac{s_0^2 (C\dot{\tilde{x}} + K\tilde{x})}{f^2 i_0 N^2 A_p \mu_0}. \quad (26)$$

Eqs. (25) and (26) were utilized to generate the control currents in MATLAB simulations. The material reluctance is omitted in the controller design but is included in the flux density calculations to derive the “actual” force in the actuator for the closed-loop simulation. This was done in order to reduce the controller’s computational demands to obtain the control currents.

Selection of effective damping and spring coefficients utilized in the controller is guided by drawing an analogy to the support motion problem in vibration theory. Small phase lags between the actual and desired motions then require small ratios of excitation frequency to natural frequency. This analogy is justified by comparison of the equations of motion.

#### 4. Simulation results

Simulations were performed with a sinusoidal reference input of 150 Hz and the target (desired) displacement. Two types of the materials are used for the rotor in the simulation: Steel and Beryllium alloy. The latter material is a high modular alloy with less than 1/3 the density of steel. The objective is to maximize the steady state axial displacement amplitude, up to  $1.27 \times 10^{-4}$  m, with the lowest possible phase lag, tracking error, and minimal  $I^2R$  power losses. The power losses per pole consisted of a DC term from the bias current and a RMS term from the resulting control currents:

$$W = i_0^2 R + (0.707|i_c|)^2 R. \quad (27)$$

The magnetic bearing design parameters shown in [Table 1](#) play an important role in determining the actuator forces and were based on constraints specific to our application. Since the flux density is saturated at 1.8 T, the maximum magnetic actuator force is limited in the simulations to

$$F_{max} = \frac{(B_{sat}f)^2 A_p N_c}{\mu_0}. \quad (28)$$

Substituting the magnetic bearing parameters from [Table 1](#) into Eq. (28), the maximum magnetic force is calculated as

$$F_{max} = 2515 \text{ N}. \quad (29)$$

Matlab simulations were completed for each type of controller in order to compare the maximum stroke, phase lag, tracking accuracy, and  $I^2R$  power losses.

Table 1  
Magnetic bearing design parameters

Parameter	Symbol	Value	Unit
Cutoff frequency of sensor	$f_s$	3000	Hz
Cutoff frequency of power amplifier	$f_{PA}$	2500	Hz
Cutoff frequency of actuator	$f_a$	1000	Hz
Mass of rotor (steel, beryllium)	$m$	22, 6	Kg
Force constant	$k$	$5.065 \times 10^{-6}$	$\text{N m}^2/\text{A}^2$
Fringe factor	$f$	0.83	
Bias current (steel, beryllium)	$i_o$	8, 4	A
Nominal air gap	$s_o$	$3.81 \times 10^{-4}$	m
Pole area	$A_p$	0.000355	$\text{m}^2$
Number of c-cores per stator half	$N_c$	4	
Number of turns	$N$	107	turns
Resistance of one of four poles	$R$	0.26	$\Omega$
Inductance of one of four poles	$L$	0.00637	H
Permeability of air	$\mu_o$	$4\pi \times 10^{-7}$	H/m
Saturation flux density	$B_{sat}$	1.8	T

#### 4.1. Tracking example with fuzzy logic controller

This simulation was performed using Simulink and its Fuzzy Logic Toolbox, with five nonlinearities from Faraday's Law, Ampere's law, Maxwell stress tensor, and power amplifier and material saturations. The membership sets and rules for this example are given in Figs. 6–9. The simulation results are given in two parts: power loss and tracking performance, which are described below.

##### 4.1.1. Power loss

The total power loss is obtained as follows. Bias current:  $i_0 = 8$  A (steel), 4.15 A (beryllium); amplitude of control current:  $|i_c| = 8$  A (steel), 3 A (beryllium). The total power loss for both stators containing a total of 8  $c$ -cores is

$$W_{steel}^{total} = 203.2 \text{ W}, \quad W_{beryllium}^{total} = 46 \text{ W}. \quad (30)$$

##### 4.1.2. Tracking performance

Fig. 11 demonstrates the tracking performance for the steel rotor and reference input with shaking amplitude of  $1.27 \times 10^{-4}$  m. The response follows the input command with little phase lag for the steel rotor. Fig. 12 shows that the simulation results for the beryllium rotor are very similar except for a slightly larger phase error.

#### 4.2. Tracking example with sliding mode controller

Tables 2 and 3 show the performance of sliding mode controllers depending on the parameters in Eqs. (19) and (20). From the tables, it is observed that the smaller  $\lambda$  becomes the lower tracking

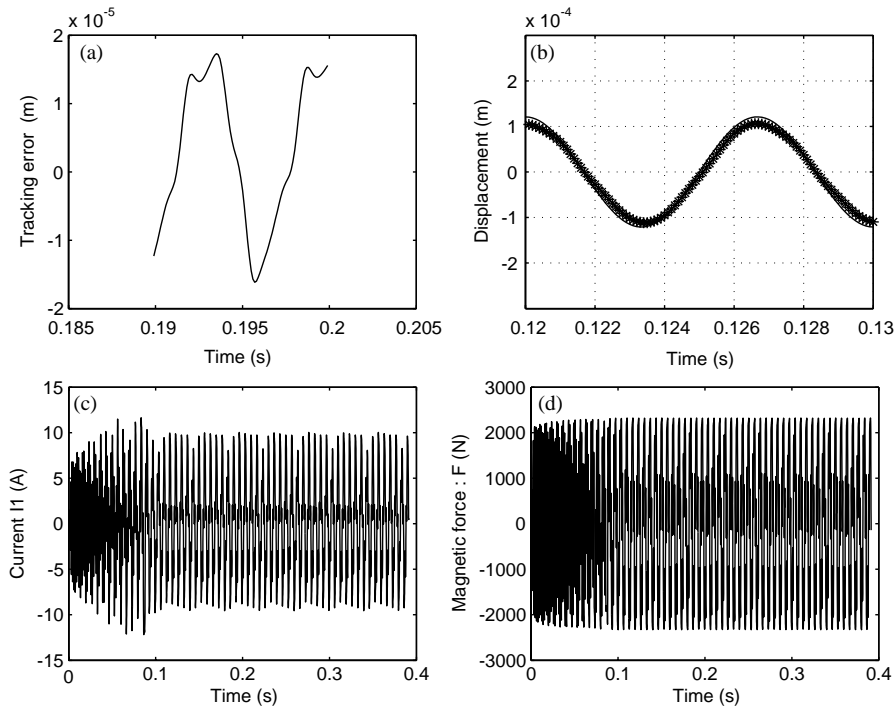


Fig. 11. (a) Tracking error, (b) displacement, (c) current and (d) force with steel shaft and fuzzy logic controller: —, input; \*, response.

error and power loss. Fig. 13 shows the tracking error, tracking response, control current, and magnetic force of the steel rotor when  $\lambda$  equal to 10 is applied. The SMC could shake up to  $1.27 \times 10^{-4}$  m with 27.7% tracking error,  $6.75^\circ$  phase lag and 188.6 W heat loss. The bias current 8 A was used while the steady state control current 7.4 A was observed. The tracking response for the beryllium rotor is shown in Fig. 14 when  $\lambda$  equal to 50 is applied. A bias current of 3.8 A was used while the steady state control current 6 A was observed. The lowest power losses for all 8 c-cores are calculated as

$$W_{steel}^{total} = 188.6 \text{ W}, \quad W_{beryllium}^{total} = 55.5 \text{ W}. \quad (31)$$

#### 4.3. Tracking example with direct linearization controller

Fig. 15 shows the response for the steel rotor with a  $1.27 \times 10^{-4}$  m, 150 Hz, sinusoidal reference input and 8 A bias current. The plot clearly shows the nearly zero phase lag with reference to the  $1.27 \times 10^{-4}$  m steady state target. The steady state control current is seen to be 7.9 A. The spring and damping coefficients were varied to determine their effect on the performance and improve controller design. The values used for Fig. 15 were  $K = 175\,880\,000$  N/m and  $C = 49\,763$  N s/m, yielding a natural frequency of 450 Hz and equivalent damping ratio of  $\zeta = 0.40$ . In practice, the damping ratio is degraded by the presence of other phase lags in the feedback path.

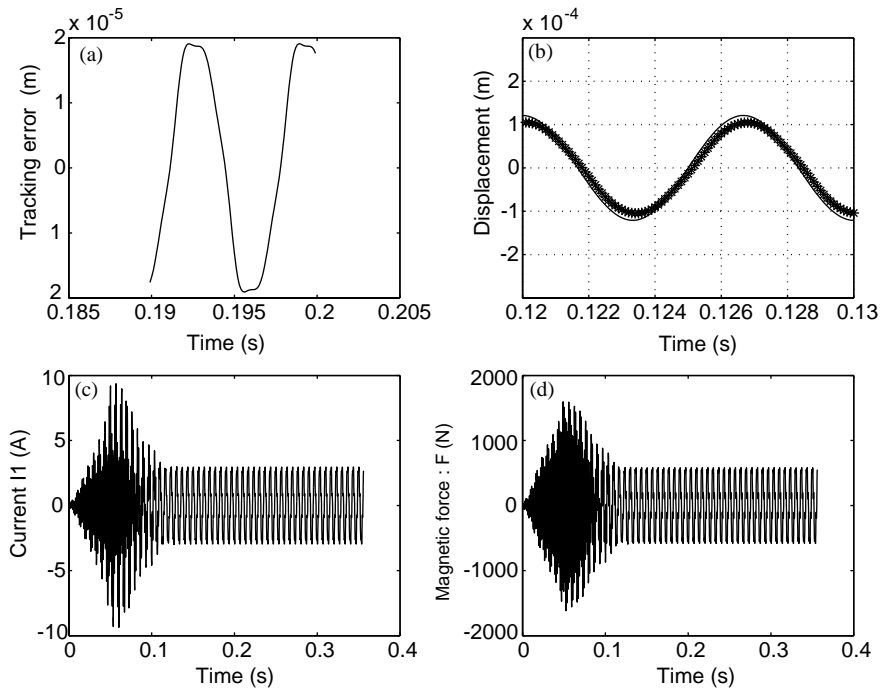


Fig. 12. (a) Tracking error, (b) displacement, (c) current and (d) force with beryllium shaft and fuzzy logic controller: —, input; \*, response.

Table 2  
Performance in steel rotor case varying  $\lambda^a$

$\lambda$	$\Phi$	Max. tracking error (m)	Phase lag (deg)	Power loss (W)
10	1.27E-3	3.49E-5	6.75	188.6
50	6.35E-3	3.55E-5	8.10	190.4
100	1.27E-2	3.65E-5	8.10	193.1
500	6.35E-2	3.88E-5	8.10	215.2
1000	2.54E-1	4.12E-5	8.10	228.4

<sup>a</sup>fixed  $\eta = 1.5$  is applied in all cases.

Table 3  
Performance in beryllium rotor case varying  $\lambda^a$

$\lambda$	$\Phi$	Max. tracking error (m)	Phase lag (deg)	Power loss (W)
50	6.35E-3	2.33E-5	2.70	55.5
100	1.27E-2	3.36E-5	$\approx 0$	55.8
500	6.35E-2	3.73E-5	2.70	57.7
1000	1.27E-1	3.55E-5	$\approx 0$	55.9

<sup>a</sup>fixed  $\eta = 23.9$  is applied in all cases.

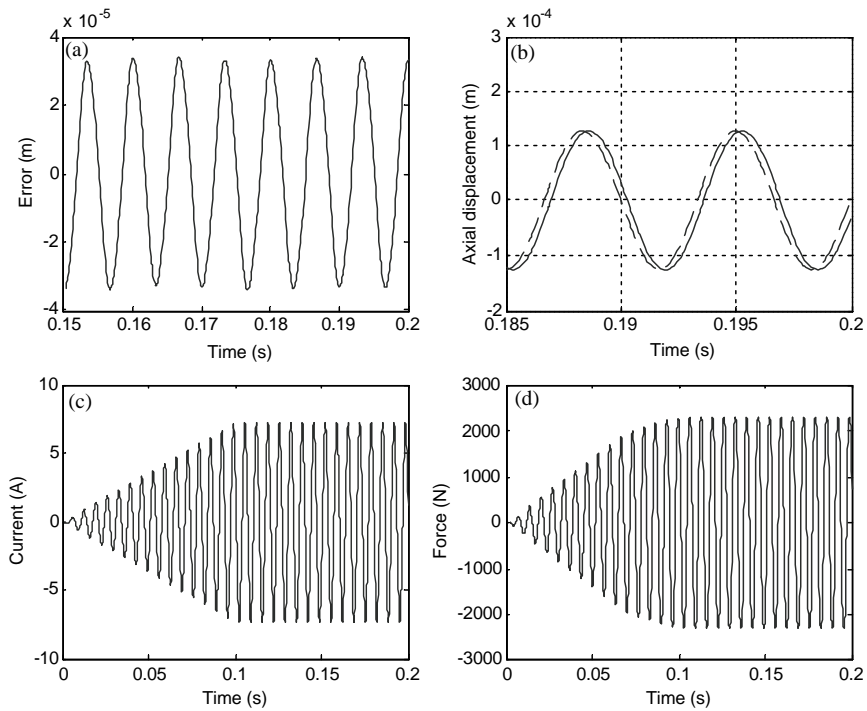


Fig. 13. (a) Tracking error, (b) displacement, (c) current and (d) force with steel shaft and sliding mode controller: ---, input; —, response.

Fig. 16 shows the results for the beryllium rotor. As expected, a  $1.27 \times 10^{-4}$  m, 150 Hz response was obtained with much lower control currents and actuator forces. The bias current was set at 4 A and the control current was 3.4 A. The reduction in power losses is the most significant benefit of the beryllium rotor. The total power losses for the 8 c-cores can be calculated from Eq. (27) as

$$W_{steel}^{total} = 198 \text{ W}, \quad W_{beryllium}^{total} = 45 \text{ W}. \quad (32)$$

The natural frequency, equivalent stiffness and damping for the beryllium rotor were 450 Hz, 47 406 000 N/m and 13 413 N s/m, respectively.

#### 4.4. Computational demand

Computation demand is an important criterion to evaluate the performance of the controllers. Fig. 17 shows the flow chart for the computation procedure of each controller. In the cases of the sliding mode and direct linearization, the conversion calculation using the non-linear magnetic equation (3) is needed while the continuous tunings of proportional P and derivative D gains using rules and membership functions are needed in the case of the fuzzy logic. For this example it was found that the fuzzy logic requires the least computational effort to provide the command

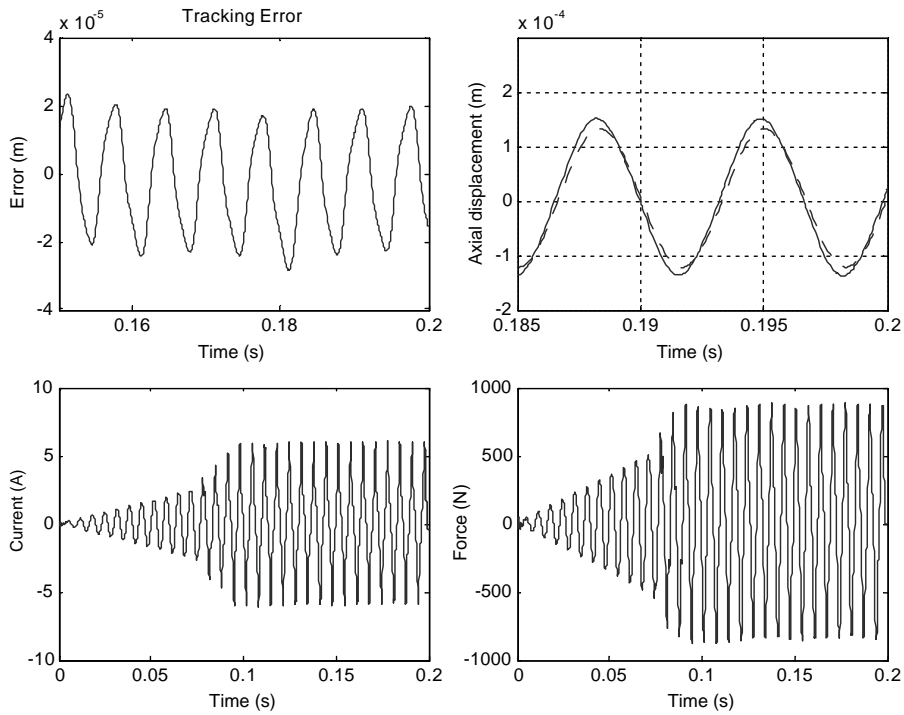


Fig. 14. (a) Tracking error, (b) displacement, (c) current and (d) force with beryllium shaft and sliding mode controller: ---, input; —, response.

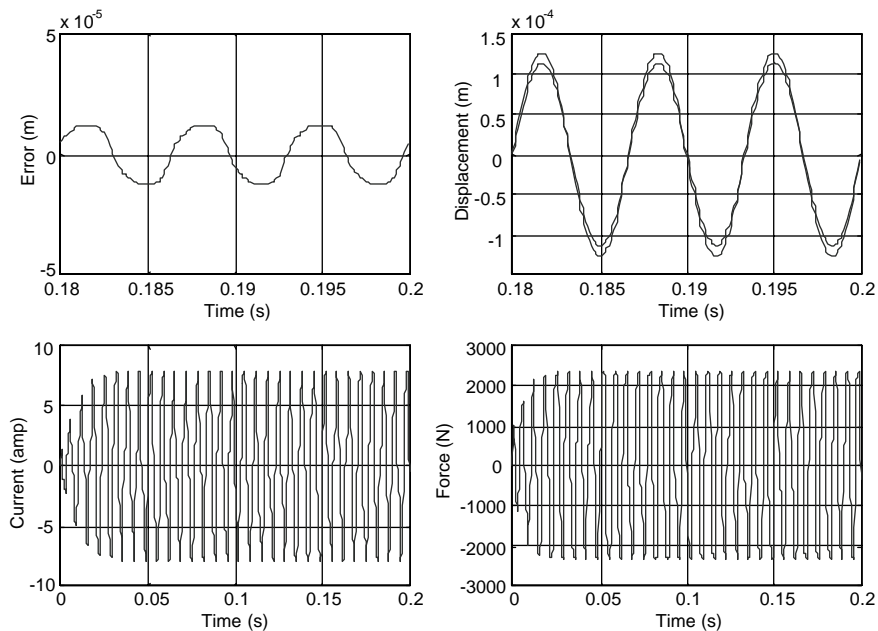


Fig. 15. (a) Tracking error, (b) displacement, (c) current and (d) force with steel shaft and direct linearization controller: —, input; ---, response.

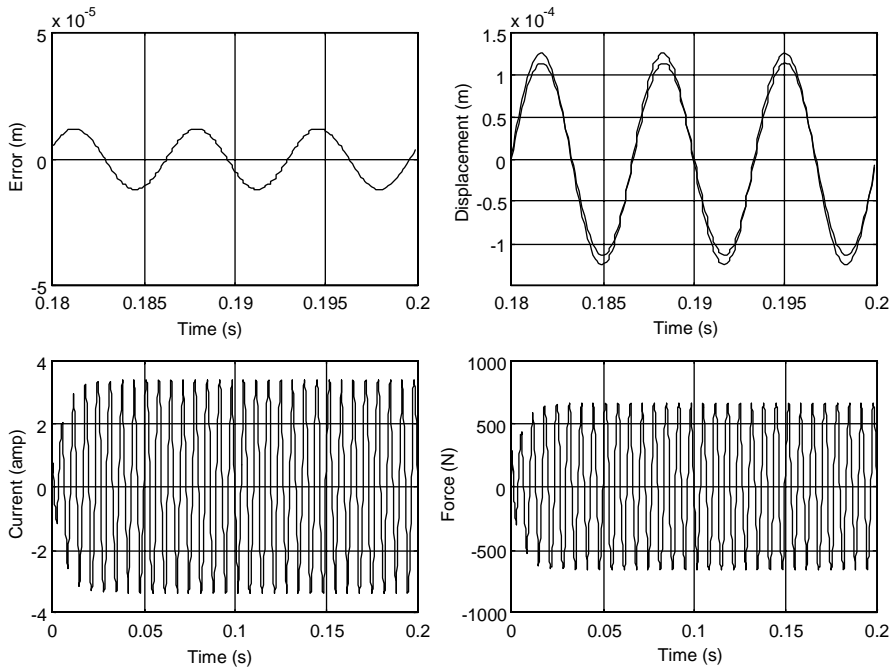


Fig. 16. (a) Tracking error, (b) displacement, (c) current and (d) force with beryllium shaft and direct linearization controller: —, input; ---, response.

voltage. This may be somewhat misleading although for actual implementation on a digital signal processor because of the time requirements to evaluate rules (Fig. 9).

#### 4.5. Performance comparison

Table 4 illustrates the performance comparison for all types of controller and for the steel and beryllium rotors.

### 5. Conclusions

This paper presents three non-linear control strategies applied to a thrust magnetic bearing to track a sinusoidal reference command. A simple linear PD controller was inadequate to shake the runner to the desired magnitude without becoming unstable, therefore non-linear controllers based on fuzzy logic, sliding mode, and direct linearization were developed. It was demonstrated that all three controllers could produce the desired magnitude of axial stroke for the rotor  $1.27 \times 10^{-4}$  m with little phase error at a frequency of 150 Hz. The amplitude error did vary with direct linearization providing the least error and sliding mode the largest error. The simulations were carried out with two types of rotor materials: steel and beryllium alloy. The beryllium alloy rotor is 3.7 times lighter than the steel rotor, which significantly reduced the total power losses with all three types of controllers. Among the three non-linear control methods, direct-linearization showed the least power consumption, phase lag, and the best tracking performance

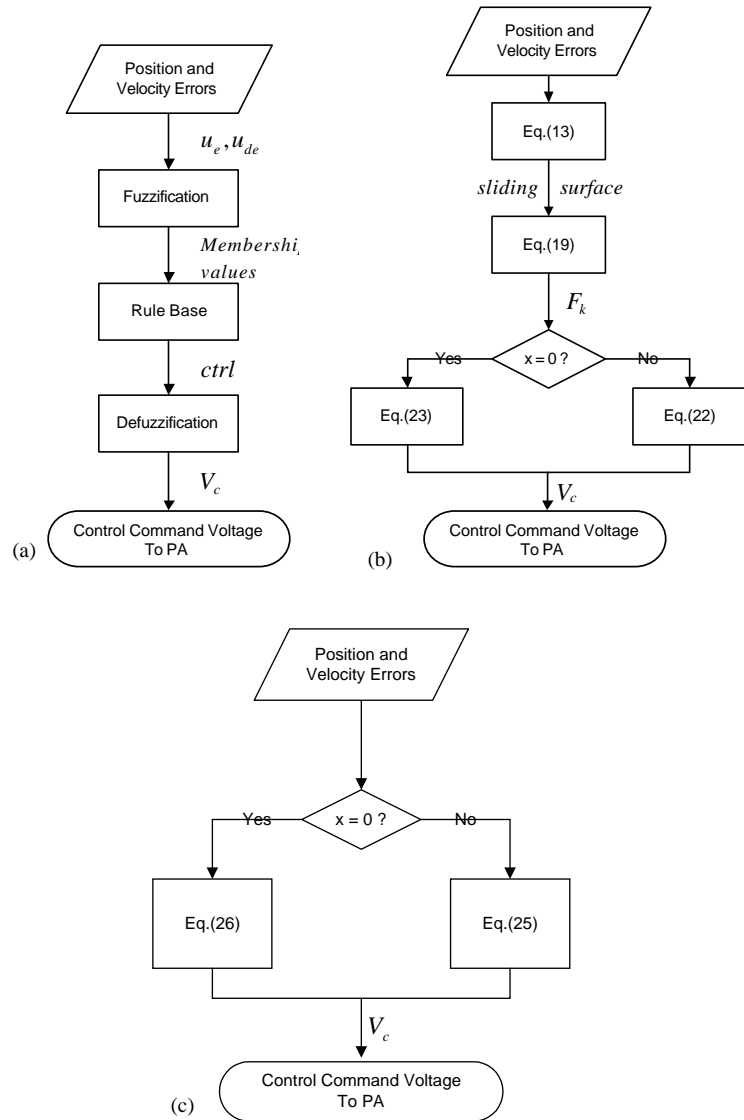


Fig. 17. Flow diagrams for computation procedure: (a) fuzzy logic, (b) sliding mode, (c) direct linearization.

and fuzzy logic the least computation demand. Future work will involve implementation of the three control strategies on a 4 hp fresh water pump and axial flow air compressor.

**Acknowledgements**

The authors gratefully acknowledge the technical and funding support for this project from the Office of NAVAL Research (Tom Calvert, Lynn Petersen and Glenn Bell) and from NASA Glenn (Gerald Montague).

Table 4  
Controller performance comparison

Performance criteria		Controller type		
		Fuzzy logic	Sliding mode	Direct linearization
Maximum axial displacement (m)	Steel	$1.27 \times 10^{-4}$	$1.27 \times 10^{-4}$	$1.27 \times 10^{-4}$
	Beryllium	$1.27 \times 10^{-4}$	$1.27 \times 10^{-4}$	$1.27 \times 10^{-4}$
Tracking error (m)	Steel	$1.80 \times 10^{-5}$	$3.49 \times 10^{-5}$	$1.25 \times 10^{-5}$
	Beryllium	$2.00 \times 10^{-5}$	$2.33 \times 10^{-5}$	$1.20 \times 10^{-5}$
Tracking error (%)	Steel	14	27.7	10.9
	Beryllium	16	19.7	10.5
Phase lag (degree)	Steel	4	6.75	0
	Beryllium	8	2.70	0
Total power losses (W)	Steel	203	188.6	198
	Beryllium	46	55.5	45
Computation demand		Low	High	Medium

## References

- [1] C. Kim, A.B. Palazzolo, et al., Eddy current effects on the design of rotor-magnetic bearing systems, *Transactions of the American Society of Mechanical Engineers* 117 (1995) 162–170.
- [2] F. Matsumura, et al., System modelling and control design of a horizontal shaft magnetic bearing system, *IEEE Transactions on Magnetics* MAG-22 (3) (1986) 196–203.
- [3] K. Nonami, et al.,  $\mu$ -Synthesis flexible rotor magnetic bearing control, *Proceedings of the International Symposium on Magnetic Bearings* 4 (1994) 73–78.
- [4] F. Carrere, et al.,  $H_\infty$  control design of flexible rotor magnetic bearings, *Proceedings of the International Symposium on Magnetic Bearings* 4 (1994) 65–72.
- [5] M. Fujita, et al., Loop shaping based robust control of a magnetic bearing, *IEEE Control System Magazine* 13 (4) (1993) 57–65.
- [6] R.D. Smith, et al., Nonlinear control of a rigid magnetic bearing system: modelling and simulation with full state feedback, *IEEE Transactions on Magnetics* 31 (2) (1995) 973–980.
- [7] Gangbing Song, et al., Integrated adaptive robust of active magnetic bearings, *Proceedings of IEEE International Conference on Systems, Man, and Cybernetics*, 1996, pp. 1784–1790.
- [8] T.-J. Yeh, et al., Sliding control of magnetic bearing systems, *American Society of Mechanical Engineers, Journal of Dynamic Systems, Measurement, and Control* 123 (2001) 353–362.
- [9] Kazuo Tanaka, et al., Model-based fuzzy control system design for magnetic bearings, *IEEE Transactions on Fuzzy Systems* (1997) 895–899.
- [10] Lih-Chang Lin, et al., Feedback linearization and fuzzy control for conical magnetic bearings, *IEEE Transactions on Control Systems and Technology* 5 (4) (1997) 417–426.
- [11] L. Zadeh, Fuzzy sets, *Information and Control* 8 (3) (1965) 338–353.
- [12] E. Mamdani, Advances in the linguistic synthesis of fuzzy controllers, *International Journals of Man–Machine Studies* 6 (1976) 669–678.
- [13] K. Tagaki, M. Sugeno, Fuzzy identification of systems and its application to modelling and control, *IEEE Transactions on Systems, Man, and Cybernetics* 15 (1985) 116–132.
- [14] J.-J.E. Slotine, et al., *Applied Nonlinear Control*, Prentice-Hall, Englewood Cliffs, NJ, 1991.